INSTITUTE OF PHYSICS PUBLISHING SMART MATERIALS AND STRUCTURES
Smart Mater. Struct. **12** (2003) 571–579 PII: S0964-1726(03)63471-3

Numerical characterization of functionally graded active materials under electrical and thermal fields

Shailendra Joshi[1], **Abhijit Mukherjee**[2,3] **and Siegfried Schmauder**[1]

[1] Staatliche Materialprüfunganstalt, Universität Stuttgart, Stuttgart-70569, Germany
[2] Department of Civil Engineering, Indian Institute of Technology, Bombay, Mumbai-400076, India

E-mail: Shailendra.Joshi@mpa.uni-stuttgart.de, abhijit@civil.iitb.ac.in and Siegfried.Schmauder@mpa.uni-stuttgart.de

Received 1 November 2002, in final form 29 April 2003
Published 25 June 2003
Online at stacks.iop.org/SMS/12/571

Abstract
This paper deals with a class of functionally graded materials (FGMs) called *active FGM* that has electro-thermo-elastically graded material phases. The focus is on the characterization of active FGM under electrical and thermal fields. The structure comprises a substrate, an electro-thermo-elastically graded layer and an active layer. Using augmented piezoelectric constitutive law, the effect of temperature on the piezoelectric properties is incorporated in the model. A formulation for exact solutions of the system based on Euler–Bernoulli theory is presented. Polynomial compositional variations of the constituent phases in the graded layer are considered and their performance for a range of stiffness and electrical property ratios of the active and substrate materials is studied under electrical and thermal fields. The effect of temperature dependence of piezoelectric coefficients on the stress distribution in the active FGM is discussed. It is also observed that the compositional variation significantly influences the actuation authority of graded materials depending on the modular ratio of the constituent materials.

(Some figures in this article are in colour only in the electronic version)

1. Introduction

Recent advances in materials science and engineering, coupled with the ubiquitous necessity to create efficient structural systems, have led to a new class of materials called functionally graded materials (FGMs). FGMs offer many advantages over monolithic materials and traditional composites. By spatially varying the microstructure, the material can be tailored for a particular application to yield optimal, thermal, electrical and mechanical behaviour. Through the use of FGMs, improved fatigue resistance, reduced thermo-electro-elastic property mismatch, interlaminar stress reduction, and more efficient joining techniques can be realized.

FGMs have received considerable attention in recent years. The primary focus has been towards the design of efficient materials suited for aerospace applications, solid oxide fuel cells and energy conversion systems using thermoelectric or thermionic materials [1]. An important application of graded materials is in tribology [2, 3] in order to improve the damage resistance of contact surfaces. Thin films with graded composition play an important role in semiconductor devices [4]. Development of FGM in defence mechanisms such as ceramic armour, thermo-nuclear suits etc is also an area of interest. Smooth transitions in compositional gradients also lead to improved bi-material bonding, allowing better mechanical integrity of the systems.

With improved functionality of graded materials, their characterization and optimization pose new challenges. In macrostructural analysis, a study of deformation and stress response of FGMs with different material phase variations in the elastic as well elasto-plastic regime is clearly warranted [5]. A comprehensive overview of the elasto-plastic

[3] Author to whom any correspondence should be addressed.

characterization of FGMs under thermal cycles can be found in [6, 7]. The response of graded materials under transient loads has been studied in order to distinguish the stress wave propagation in graded materials from layered materials [8, 9]. In [9] a semi-empirical numerical model was developed to include strain-rate effects in the elastic and visco-plastic response. In the microstructural characterization of FGM, combined experimental–numerical investigations have been carried out to determine the material parameters such as elastic and plastic properties and fracture toughness [10–12]. Inverse techniques based on neural network and genetic algorithms have also been proposed to characterize graded materials [13, 14]. Exhaustive micromechanical simulations have been performed on periodic and random FGM microstructures in order to derive effective properties and behaviour under prescribed thermo-mechanical excitations [15–18]. Recently, elasto-plastic stress solutions for thermo-elastic FGMs have been presented using a self-consistent approach [19].

One class of FGM, which is the focus of this paper, is electro-elastic FGM (active FGM), in that the electro-elastic mismatch between constituent material phases is minimized through continuous gradation. In the present context, an active FGM comprises ferroelectric or, in particular, piezoelectric material as one of the material phases. Such materials find use in electro-mechanical devices, popularly known as *smart systems*. Functionally graded transducers have potential applications in ultra-sonic medical imaging where broadband frequency characteristics (short pulse emission) are desirable. Conventional thin piezoelectric transducers are limited due to narrow-band frequency characteristics on account of the pulses being emitted at both the surfaces [20].

Active FGM is a nascent area of research. However, the design of a multi-layered actuator in [21] indicates the importance of functionally graded piezoelectric materials in practical applications. The reader may refer to [22] and [23] for the process development of a typical active FGM. Early notable work in this area includes numerical investigations on the nature of surface waves in piezoelectric FGM plates [24, 25]. Analytical studies are focused mainly on either elastic or electrical gradation [26–30]. In [26] microdisplacement and microstructure characteristics of graded piezoelectric materials have been reported. Few researchers have studied controlled responses of functionally graded plates with bonded actuators [27, 28]. In these cases, only elastic gradation is considered. In [29] exact solutions are derived for electrically graded monomorphs. The results indicate the strong influence of electrical gradation on the stress characteristics and electric field. Numerical investigations for FGM bimorphs have been reported [30] for linear and nonlinear gradation to maximize displacement of the actuator while minimizing the maximum stress.

The present literature on FGM primarily focuses either on thermo-elastic or electro-elastic gradations. It is well-known that the electrical properties of the piezoelectric materials are influenced by temperature [31, 32], e.g. their depolarization is signified by Curie temperature. Few recent works have been carried out that consider micromechanics of coupled thermo-electro-magneto-elastic materials [33, 34]. It is desirable, however, to provide a simple phenomenological model incorporating thermal as well as electrical compositional gradation.

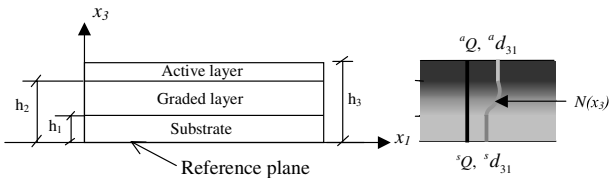

Figure 1. Layer structure and property gradation of an electro-elastically graded material.

In this paper, we develop an augmented uniaxial model based on [31] for electro-thermo-elastically graded materials. It includes the influence of the thermal field on the electrical properties of the active material. Using Euler–Bernoulli theory, exact solutions are presented for obtaining the response of active FGM to electrical and thermal excitations. The material distribution may be symmetric or asymmetric about the reference plane. Using the modified relations, the through-thickness stress distributions under electrical and thermal fields are studied.

In the available literature on FGM, the power-law-type compositional gradation has frequently been employed. The performance of this type of grading is evaluated *vis-à-vis* a complete polynomial-type grading. The piezoelectric active layers with several substrate–active material ratios of practical interest are considered. The expressions for both actuator and sensor are presented. The performance of the actuator is also studied. We restrict the scope of this investigation to low electric fields and thermal excitations that are well below the Curie temperatures. In other words, the present analysis does not consider the nonlinearities arising from domain switching and depolarization due to high electric fields and thermal effect.

2. Material system

The material comprises a piezoelectric layer, a graded layer and a substrate (figure 1). The material may be stacked symmetrically or asymmetrically with respect to the reference plane. The variation of material properties over FGM thickness is defined as

$$P(x_3) = ({}^sP + \Delta P N(x_3)) \tag{1}$$

where, $\Delta P = ({}^sP - {}^aP)$, ${}^sP$ and ${}^aP$ are the material properties of the substrate and the active layer and the function $N(x_3)$ is the compositional variation of the active material in the graded layer. The augmented linear constitutive relations for electro-elastically graded materials are defined as

$$\sigma_{ij} = Q_{ijkl}(\varepsilon_{kl} - d_{klm}E_m - \bar{d}_{klm}E_m\Delta T - \alpha_{ij}\Delta T) \tag{2}$$

$$D_m = d_{kji}Q_{ijkl}\varepsilon_{kl} + \bar{d}_{kji}Q_{ijkl}\varepsilon_{kl}\Delta T + \xi_{km}E_m + \bar{\xi}_{km}E_m\Delta T + p_m\Delta T \tag{3}$$

where σ_{ij} is the second-order stress tensor, Q_{ijkl} is the fourth-order stiffness tensor as a function of the thickness of material, (x_3) ε_{ij} is the second-order strain tensor, d_{klm} is the third-order piezoelectric strain tensor as a function of x_3, D_m is the electric displacement vector, ξ_{km} is the second-order permittivity tensor as a function of x_3, E_m is the electrical field vector, p_m is the pyroelectric coefficient vector, and ΔT is the change in temperature from the reference state (that is, a state free of thermal residual stress).

Equations (2) and (3) represent the modified converse and the direct piezoelectric effects to include the temperature dependence of piezoelectric properties through terms $\bar{d}_{klm}$ and $\bar{\xi}_{km}$. These properties have been shown to be relatively independent of the electric field level [31].

For a structure with a length that is large compared to its width and thickness, the Euler–Bernoulli theory can be used for the solutions at all locations away from the edges. Further, if the voltage is applied across the thickness, then the electrical field is generated only in the x_3-direction and is denoted by E_3. We also assume that a uniform temperature difference (ΔT) is applied over the material thickness only. For such a case, equation (2) reduces to

$$\sigma_1 = Q_{11}[\varepsilon_1 - (d_{31} + \bar{d}_{31}\Delta T)E_3 - \alpha \Delta T] \tag{4}$$

where σ_1, ε_1 and Q_{11} are the stress, strain and elastic modulus, d_{31} and $\bar{d}_{31}$ are the piezoelectric strain coefficients in the x_1-direction, while the electric field is in the x_3-direction and α is the coefficient of thermal expansion. Similarly, the direct piezoelectric equation is simplified to

$$D_3 = Q_{11}(d_{31}\varepsilon_1 + \bar{d}_{31}\varepsilon_1 \Delta T) + (\xi_{33} + \bar{\xi}_{33}\Delta T)E_3 + p_3 \Delta T. \tag{5}$$

The strain at any point (ε_1) can be expressed in terms of strain at the reference plane as follows:

$$\varepsilon_1 = \varepsilon_0 - x_3\kappa \tag{6}$$

where ε_o is the in-plane strain and κ is the curvature.

Noting that the piezoelectric properties now include temperature effects and using the variable definitions from figure 1, the constitutive relations in equations (4) and (5) can be elaborated as

$$\sigma_1(x_3) = ({}^sQ_{11} + \Delta Q N(x_3)\gamma)[\varepsilon_o - x_3\kappa - ({}^sd'_{31} + \Delta d'_{31}N(x_3)\gamma)E_3 - ({}^s\alpha + \Delta\alpha N(x_3)\gamma)\Delta T] \tag{7}$$

and

$$D_3(x_3) = [({}^sQ_{11} + \Delta Q N(x_3)\gamma)({}^sd'_{31} + \Delta d'_{31}N(x_3)\gamma) \times (\varepsilon_o - x_3\kappa)] + ({}^s\xi'_{33} + \Delta\xi'_{33}N(x_3)\gamma)E_3 + p_3\Delta T \tag{8}$$

where ${}^sQ_{11}$ and ${}^aQ_{11}$ are the elastic moduli, ${}^sd'_{31}$ and ${}^ad'_{31}$ are the piezoelectric strain coefficients, and ${}^s\xi'_{33}$ and ${}^a\xi'_{33}$ are the permittivity coefficients of the substrate and the active material, respectively. The prime indicates that the electrical properties are temperature dependent. The mismatches are given as $\Delta Q = ({}^aQ_{11} - {}^sQ_{11})$, $\Delta d_{31} = ({}^ad'_{31} - {}^sd'_{31})$, $\Delta\xi_{33} = ({}^a\xi'_{33} - {}^s\xi'_{33})$, and $\Delta\alpha = ({}^a\alpha - {}^s\alpha)$. The parameter γ is defined as

$$\gamma = \begin{cases} 0 & 0 \leqslant |x_3| \leqslant |h_1| \\ 1 & |h_1| \leqslant x_3 \leqslant |h_2|,\ |h_2| \leqslant x_3 \leqslant |h_3| \end{cases} \tag{9}$$

where $|\cdot|$ represents the magnitude of the ordinate.

Using the converse piezoelectric effect, the force and bending moment equilibrium equations can be obtained from the following expressions:

$$\int_0^{h_3} \sigma_1(x_3)\,\mathrm{d}x_3 = 0; \qquad \int_0^{h_3} x_3\sigma_1(x_3)\,\mathrm{d}x_3 = 0. \tag{10}$$

Integrating equation (10), the strain components ε_o and κ are given as follows:

$$\boldsymbol{K}\varepsilon + \boldsymbol{B} = 0 \tag{11}$$

where $\boldsymbol{K}$ is a 2×2 matrix of rigidity coefficients, $\varepsilon = (\varepsilon_o - \kappa)^{\mathrm{T}}$ is the vector of strains, and $\boldsymbol{B} = (b_1 b_2)^{\mathrm{T}}$ is the vector of body forces developed due to applied electrical and thermal fields. The terms in $\boldsymbol{K}$ and $\boldsymbol{B}$ are defined as

$$k_{11} = \sum_{i=1}^{m}[{}^sQ_{11}h_1 + {}^sQ_{11}(h_2 - h_1) + \Delta Q I_1 + {}^aQ_{11}(h_3 - h_2)] \tag{12}$$

$$k_{12} = k_{21} = \sum_{i=1}^{m}\left[\frac{{}^sQ_{11}h_1^2}{2} + \frac{{}^sQ_{11}(h_2^2 - h_1^2)}{2} + \Delta Q I_2 + \frac{{}^aQ_{11}(h_3^2 - h_2^2)}{2}\right] \tag{13}$$

$$k_{22} = \sum_{i=1}^{m}\left[\frac{{}^sQ_{11}h_2^3}{3} + \frac{{}^sQ_{11}(h_2^3 - h_1^3)}{3} + \Delta Q I_5 + \frac{{}^aQ_{11}(h_3^3 - h_2^3)}{3}\right] \tag{14}$$

$$b_1 = \sum_{i=1}^{m}[{}^sQ_{11}[E_3({}^sd'_{31}h_1 + {}^sd'_{31}(h_2 - h_1) + \Delta d'_{31}I_1) + \Delta T({}^s\alpha h_1 + {}^s\alpha(h_2 - h_1) + \Delta\alpha I_1)] + \Delta Q[E_3({}^sd'_{31}I_1 + \Delta d'_{31}I_3) + \Delta T({}^s\alpha I_1 + \Delta\alpha I_3)] + {}^aQ_{11}[{}^ad'_{31}E_3(h_3 - h_2) + {}^a\alpha\Delta T(h_3 - h_2)]] \tag{15}$$

$$b_2 = \sum_{i=1}^{m}\left[\frac{{}^sQ_{11}}{2}[E_3({}^sd'_{31}h_1^2 + 2\Delta d'_{31}I_4) + \Delta T({}^s\alpha h_1^2 + 2\Delta\alpha I_4)] + \Delta Q[E_3(d^s_{31}I_4 + \Delta d'_{31}I_6) + \Delta T({}^s\alpha I_4 + \Delta\alpha I_6)] + \frac{{}^aQ_{11}}{2}[{}^ad'_{31}E_3(h_3^2 - h_2^2) + {}^a\alpha\Delta T(h_3^2 - h_2^2)]\right]. \tag{16}$$

The integral terms (I_1–I_6) in equations (12)–(16) depend on the compositional gradation.

For the direct piezoelectric effect, using Gauss' law for electrodes in short-circuit, the induced charge (q) due to applied strain is given as

$$q = \left[\int\int_A D_3\,\mathrm{d}A\right] \tag{17}$$

where the electric displacement is

$$D_3 = \int_{x_3} D_3(x_3)\,\mathrm{d}x_3. \tag{18}$$

The capacitance of the material is

$$C = \frac{1}{h}\int_A\left(\int_{x_3}({}^s\xi'_{33} + \Delta\xi'_{33}N(x_3)\gamma)\,\mathrm{d}x_3\right)\mathrm{d}A \tag{19}$$

where h is the distance between the two electrode surfaces and A is the plan area of electrodes common to both faces of the material. The induced voltage (V) is

$$V = \frac{q}{C}. \tag{20}$$

3. Compositional variations

In this work, two gradation functions [$N(x_3)$] are considered. They are defined in terms of the volume fraction of the active

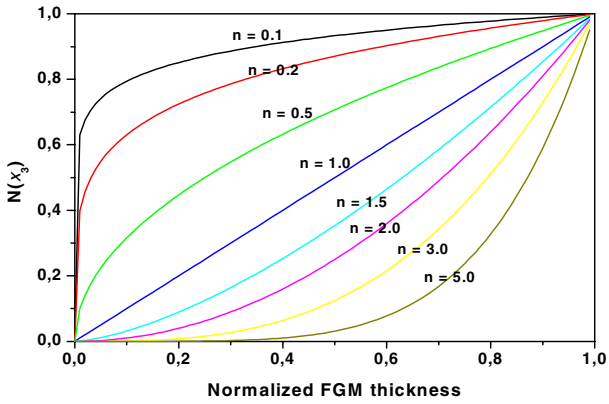

Figure 2. Power-law variation of electro-elastic properties in the FG layer.

material in the graded layer. In the first case, a power-law function (figure 2) is considered as

$$N(x_3) = \left(\frac{x_3 - h_1}{h_2 - h_1}\right)^n. \tag{21}$$

As the gradation function in equation (21) is bounded by the parameter γ defined in equation (9), we have

$$N(x_3) = \begin{cases} 0 & @\ x_3 = h_1 \text{ and } -h_1 \\ 1 & @\ x_3 = h_2 \text{ and } -h_2. \end{cases} \tag{22}$$

The integral terms (I_1–I_6) in equations (12)–(16) for the power-law-type gradation are obtained explicitly and are given as follows:

$$I_1 = \int_{h_1}^{h_2} N(x_3)\,\mathrm{d}x_3 = \frac{1}{(h_2 - h_1)^n}\left[\frac{(h_2 - h_1)^{n+1}}{n+1}\right] \tag{23a}$$

$$I_2 = I_4 = \int_{h_1}^{h_2} N(x_3)x_3\,\mathrm{d}x_3 = \frac{1}{(h_2 - h_1)^n}\left[\frac{(h_2 - h_1)^{n+2}}{n+2} - \frac{h_1(h_2 - h_1)^{n+1}}{n+1}\right] \tag{23b}$$

$$I_3 = \int_{h_1}^{h_2} (N(x_3))^2\,\mathrm{d}x_3 = \frac{1}{(h_2 - h_1)^{2n}}\left[\frac{(h_2 - h_1)^{2n+1}}{2n+1}\right] \tag{23c}$$

$$I_5 = \int_{h_1}^{h_2} N(x_3)x_3^2\,\mathrm{d}x_3 = \frac{1}{(h_2 - h_1)^n}\left[\frac{(h_2 - h_1)^{n+3}}{n+3} + h_1\frac{(h_2 - h_1)^{n+2}}{n+2} + h_1^2\frac{(h_2 - h_1)^{n+1}}{n+1}\right] \tag{23d}$$

$$I_6 = \int_{h_1}^{h_2} (N(x_3))^2 x_3\,\mathrm{d}x_3 = \frac{1}{(h_2 - h_1)^{2n}}\left[\frac{(h_2 - h_1)^{2n+2}}{2n+2} + h_1\frac{(h_2 - h_1)^{2n+1}}{2n+1}\right]. \tag{23e}$$

In the second case, a generalized cubic-shape function is considered as follows:

$$N(x_3) = a + b\left(\frac{x_3 - h_1}{h_2 - h_1}\right) + c\left(\frac{x_3 - h_1}{h_2 - h_1}\right)^2 + d\left(\frac{x_3 - h_1}{h_2 - h_1}\right)^3. \tag{24}$$

In addition to the boundary conditions in equation (22),

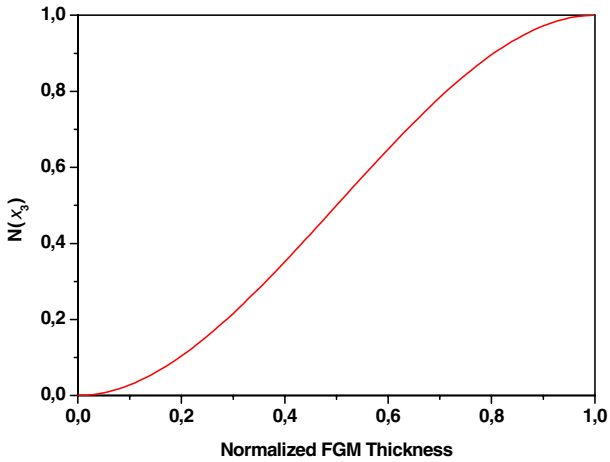

Figure 3. CG2 variation of electro-elastic properties in the FG layer.

constraints are put on the gradient of the function as follows:

$$\frac{\mathrm{d}N(x_3)}{\mathrm{d}x_3} = \begin{cases} 0 & @\ x_3 = h_1 \text{ and } -h_1 \\ 0 & @\ x_3 = h_2 \text{ and } -h_2. \end{cases} \tag{25}$$

Substituting $\eta = (\frac{x_3 - h_1}{h_2 - h_1})$, where $0 \leqslant \eta \leqslant 1$, therefore

$$N(\eta) = a + b\eta + c\eta^2 + \mathrm{d}\eta^3 \tag{26}$$

$$\frac{\mathrm{d}N(\eta)}{\mathrm{d}\eta} = b + 2c\eta + 3\,\mathrm{d}\eta^2. \tag{27}$$

Using equations (26) and (27), a set of simultaneous equations can be written as

$$\begin{bmatrix} 1 & \eta & \eta^2 & \eta^3 \\ 0 & 1 & \eta & \eta^2 \\ 1 & \eta & \eta^2 & \eta^3 \\ 0 & 1 & \eta & \eta^2 \end{bmatrix} \begin{Bmatrix} a \\ b \\ c \\ d \end{Bmatrix} = \begin{Bmatrix} 0 \\ 0 \\ 1 \\ 0 \end{Bmatrix}. \tag{28}$$

Solving equation (28), we obtain a cubic gradation with controlled interfacial gradients (CG2) (figure 3):

$$N(\eta) = (3\eta^2 - 2\eta^3). \tag{29}$$

For the CG2, the integral terms are explicitly evaluated as follows:

$$I_1 = \frac{(h_2 - h_1)}{2} \tag{30a}$$

$$I_2 = I_4 = (h_2 - h_1)\left\{\frac{7(h_2 - h_1)}{20} + \frac{h_1}{2}\right\} \tag{30b}$$

$$I_3 = \tfrac{13}{35}(h_2 - h_1) \tag{30c}$$

$$I_5 = (h_2 - h_1)\left\{\frac{4(h_2 - h_1)^2}{15} + \frac{14(h_2 - h_1)h_1}{20} + \frac{h_1^2}{2}\right\} \tag{30d}$$

$$I_6 = (h_2 - h_1)\left[\left(\frac{9h_1}{5} + \frac{9(h_2 - h_1)}{6}\right) - \left(2h_1 + \frac{12(h_2 - h_1)}{7}\right) + \left(\frac{4h_1}{7} + \frac{(h_2 - h_1)}{2}\right)\right]. \tag{30e}$$

In equations (12)–(16), the reference plane is located at the bottom surface of the substrate material (figure 1). Two

possibilities are considered in the present set of expressions. The first one is that the material is stacked entirely above the reference plane ($m = 1$) in three layers, namely substrate, FG layer and active layer. The second possibility is that the material is stacked symmetrically about the reference plane, the symmetry being in terms of both geometry and material properties ($m = 2$). It may be noted that equations (23*a*)–(23*e*) and (30*a*)–(30*e*) are derived for positive x_3-coordinate. Similar expressions can be obtained for negative x_3-coordinate if the material is distributed symmetrically below the reference plane. The terms ε_o and κ are obtained by solving equation (11). Once the solution for ε_o and κ is available, the transducer characteristics of the material can be obtained by using equations (7), (8) and (20).

4. Results and discussion

Based on the explicit expressions given in section 3, solutions for electro-thermo-elastically graded material are sought for different stimuli. The results are organized in three parts as follows:

(1) electro-elastic FGM subjected to electric field;
(2) electro-thermo-elastic FGM subjected to combined electric and thermal fields;
(3) the effect of temperature-dependent electric properties on the characteristics of graded material.

4.1. Electro-elastic FGM subjected to electric field

In this part, the influence of different electro-elastic gradations on the stress distribution in the material under electrical excitations is analysed. We neglect the thermal terms in the equations derived in section 2. For the sake of comparison, linear and cubic power-law gradations are considered along with the cubic grading with controlled gradients (CG2). Keeping the piezoelectric mismatch (Δd_{31}) constant, modular ratios (${}^sQ_{11}/{}^aQ_{11}$) ranging between 0.05–10.0 are considered in order to cover a broad range of constituent phases. Unless otherwise specified, the substrate is assumed to be electrically inactive (${}^sd_{31} = 0$).

To characterize the material, a symmetric layer structure of the constituents has been considered. In a symmetrical composite the in-plane strain ε_o and the curvature κ (equation (11)) can be created separately. When an electrical field of the same magnitude and polarity is applied, only in-plane strain exists. Only curvature is created through the application of equal electrical fields but with opposite polarities about the plane of symmetry. In the framework of small deformation theory, a superposition of both cases gives the response of the material subjected to an arbitrary electrical field. In all the cases, an electrical field inducing a strain (${}^ad_{31}E_3$) of 100 $\mu\varepsilon$ is applied. It is to be noted that the force applied will be different for different compositional gradations. The stress variation is plotted as a non-dimensional ratio of the axial stress to the stress induced in a pure piezoelectric material (${}^aQ_{11}{}^ad_{31}E_3$). This leads to a qualitative description of the stress variation that is independent of the material properties and induced strain.

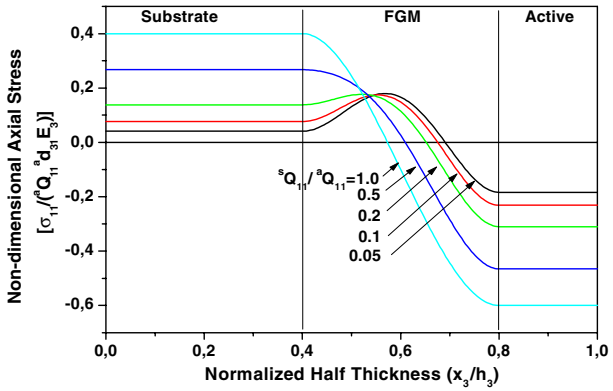

a. CG2

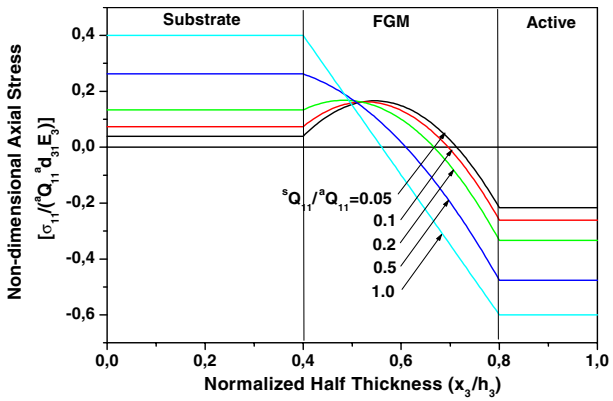

b. Linear gradation

Figure 4. Non-dimensional in-plane stresses due to electric fields of the same polarity (${}^sQ_{11}/{}^aQ_{11} \leqslant 1.0$).

4.1.1. Example 1: In-plane strain. Figures 4(a), (b) and 5(a), (b) show a comparison between the stress characteristics for linear ($n = 1$) and CG2 FGMs subjected to a pure membrane strain. The advantage of controlling the gradients of the gradation profile is clearly visible from the comparison of the stress profiles for the linear and cubic variations. Sharp cusps at the interfaces of the FG layer are completely eliminated and the stress distribution is smoother.

Further, the CG2 results in stress reduction at the interface between the FG layer and the stiffer layer. The maximum reduction in the stress occurs for extreme modular ratios, and it is about 16% for modular ratio 0.05 (figure 6).

The CG2 not only results in reduced stresses but also minimizes the maximum stress gradient, resulting in better overall stress distribution in the material. In figure 7, zero stress gradients at both the interfaces in the case of CG2 indicate smooth stress distribution. Linear grading results in discontinuity in the slope of the stress distribution at both interfaces, whereas cubic power-law grading possesses high stress gradient at the FG–active layer interface. The CG2 leads to about 17% reduction in the stress gradient over linear FGM and nearly 72% reduction compared to the cubic power-law FGM. Albeit smooth, a high-order power law performs poorly because the nature of grading results in an undesirably sharp transition in the material characteristics over a small region in the FG layer (figure 2). For CG2, the maximum stress gradient occurs at 0.75 times the thickness of the FG layer, whereas the gradient is highest at the FG–stiff layer interface for a power-law FGM.

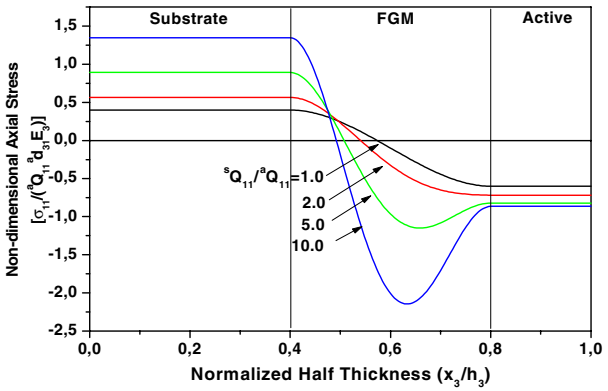

a. CG2

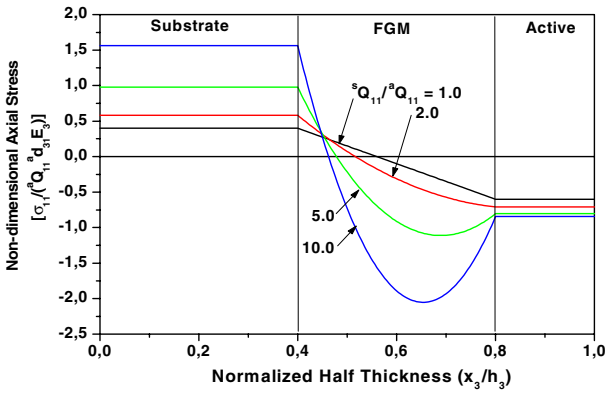

b. Linear

Figure 5. Non-dimensional in-plane stresses due to electric fields of the same polarity (${}^{s}Q_{11}/{}^{a}Q_{11} \geqslant 1.0$).

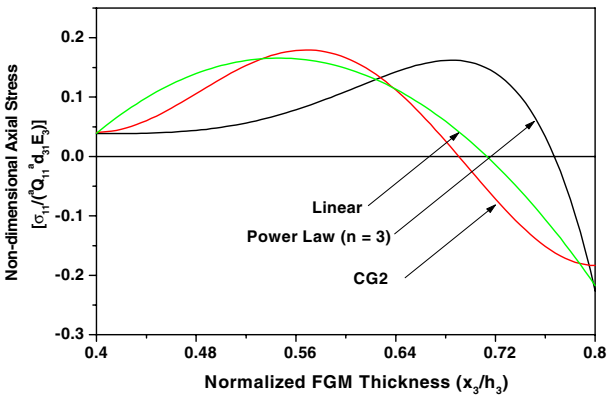

Figure 6. A comparison of axial stresses for the modular ratio 0.05.

4.1.2. Example 2: Curvature strain. Figures 8(a) and (b) and 9(a) and (b) present the non-dimensional stress distribution due to the application of electrical fields with opposite polarities in the active layers. In this case a pure curvature is produced in the material, characterized by linear variation of stresses in the non-FG layers. In the FG layer, however, the variation is non-linear. All the observations made in the case of the previous example are also valid here.

4.1.3. Example 3: Actuation authority of different compositional variations. It is imperative to study the actuation characteristics of active FGM under an induced electrical field. The linear and CG2 compositional variations

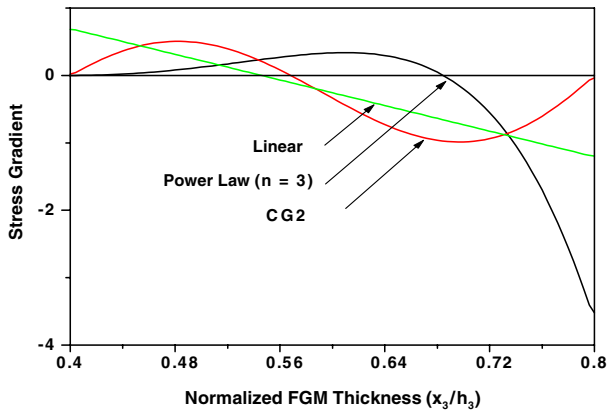

Figure 7. A comparison of stress gradients in the FG layer for the modular ratio 0.05.

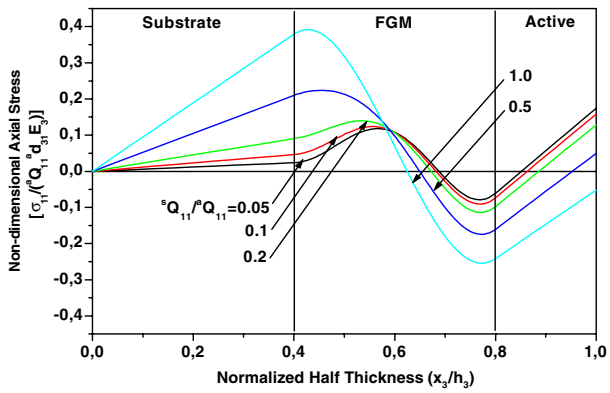

a. CG2

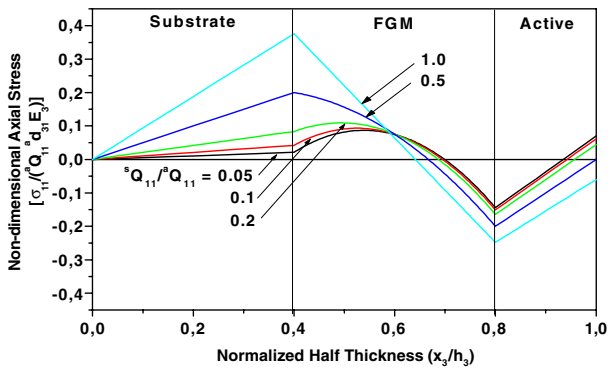

b. Linear

Figure 8. Non-dimensional in-plane stresses due to electric fields of opposite polarity (${}^{s}Q_{11}/{}^{a}Q_{11} \leqslant 1.0$).

are considered in order to study their ability to produce actuation. It is to be noted that the CG2 variation is anti-symmetric about the linear variation. Therefore, for a given modular ratio and thickness, the stiffnesses of the two systems are equal. This allows easy comparison of their actuation characteristics. If the force induced by one of the gradations is more than the other, then it can be deduced logically that the induced strain will also be higher, indicating higher actuation capability of that gradation.

Figure 10 gives the comparison of the in-plane as well as curvature actuation authorities of CG2 FGM *vis-à-vis* linear gradation under the same electrical field. It is interesting to

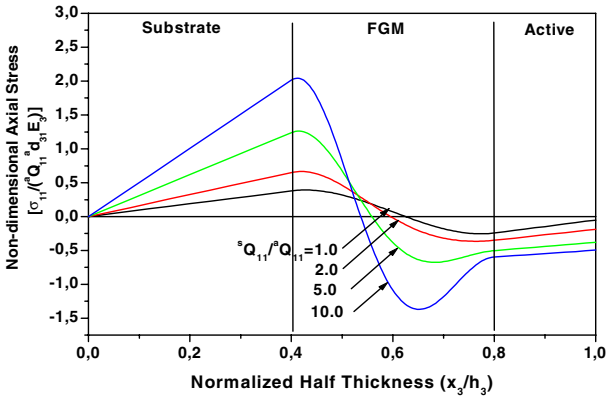

a. CG2

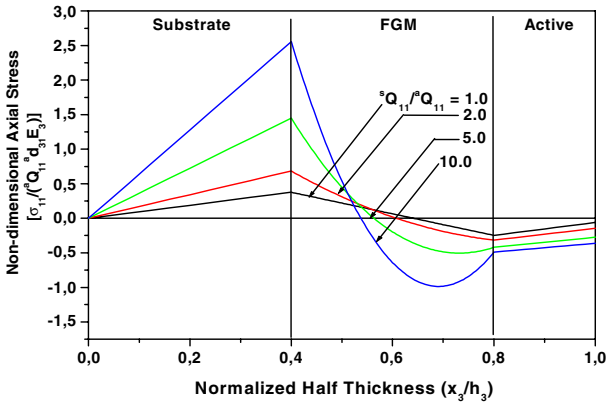

b. Linear

Figure 9. Non-dimensional in-plane stresses due to electric fields of opposite polarity (${}^{s}Q_{11}/{}^{a}Q_{11} \geqslant 1.0$).

note that the actuation authority is not only influenced by compositional variation but also by the modular ratio. If the modular ratio is less than one (soft substrate), then CG2 gradation shows marginally higher actuation authority than the linear gradation. Likewise, if the ratio is higher than one (stiff substrate), then the linear compositional variation shows significant improvement in actuation capability. This behaviour can be explained through detailed calculations of the force terms in equations (15) and (16). Such behaviour is a combined effect of the piezoelectric and elastic mismatch and the integral effect that comes from the type of compositional variation. In this case study it so happens that for modular ratios greater than one the combined effect of the above parameters is additive for linear grading, whereas in the case of the CG2 grading these parameters oppose each other. To this end, it becomes an interesting problem to solve for an ideal compositional gradation that minimizes interfacial stress gradients and maximizes the actuation characteristics.

4.2. Electro-thermo-elastic FGM subjected to combined electric and thermal fields

We now include the thermal effect in the characterization. Typically, materials are processed at a stress-free temperature (also termed the reference temperature). However, the operating temperatures may be different to the reference temperature and lead to thermal stresses in the material. It is thus necessary to include their effect in order to characterize

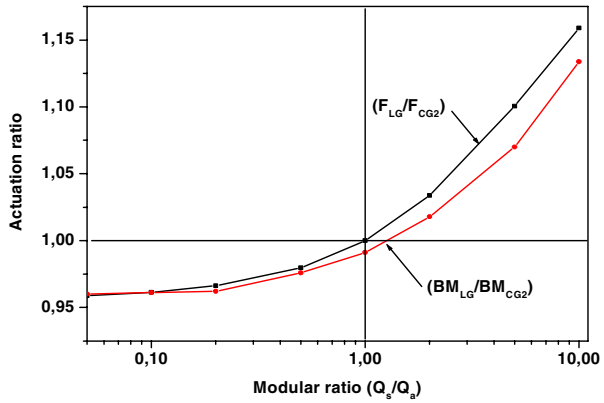

Figure 10. Actuation authorities of the linear (LG) and the CG2 compositional gradations for different modular ratios.

Table 1. Material properties.

	Ni	PZT5H
Elastic modulus, Q_{11} (GPa)	214.0	67.0
Thermal coefficient, α ($^{\circ}C^{-1}$)	15.4×10^{-6}	7×10^{-6}
Piezoelectric coefficient, d_{31} (m V^{-1})	—	-274×10^{-9}
Dielectric coefficient, ξ_{33} (F m^{-1})	—	15×10^{-9}

them correctly. In this subsection we consider a three-layered system comprising a PZT5H ceramic as the active phase, nickel (Ni) as the substrate, and a thermo-electro-elastically graded layer. The material is assumed to be stress-free at room temperature (25 °C). The properties of constituent materials are given in table 1. The thickness of the FG layer is taken to be twice the thickness of the substrate. The substrate and active layers have the same thickness.

The material is subjected to an electrical field, causing electrical strain of 100 $\mu\varepsilon$, and the ambient temperature is 15 °C, resulting in a cooling effect with a uniform temperature difference (ΔT) equal to -10 °C. In the present example, the direction of the applied electrical field is such that it minimizes the stresses induced due to the thermal effect. The stresses induced for different compositional variations are shown in figure 11. It is to be noted that a combined in-plane and curvature effect is induced due to the asymmetric nature of the layer structure. Owing to the phenomenological simile between the electrical and the thermal terms, the piezoelectric effect can be adopted as a mechanism to counter the thermal stresses that occur in materials that operate under temperatures away from their stress-free state. Conversely, it also means that the control effect due to piezoelectricity will be significantly influenced in the presence of a thermal field. Of course, this phenomenon will also hold true in materials that do not have a graded interface between the substrate and the active layer. However, the presence of a graded layer will always ensure that there is no stress discontinuity occurring under either electrical, thermal or combined electro-thermal fields.

4.3. Thermally dependent piezoelectric effects

Finally, we include the thermal dependence of piezoelectric strain coefficients in the model and study the changes in the

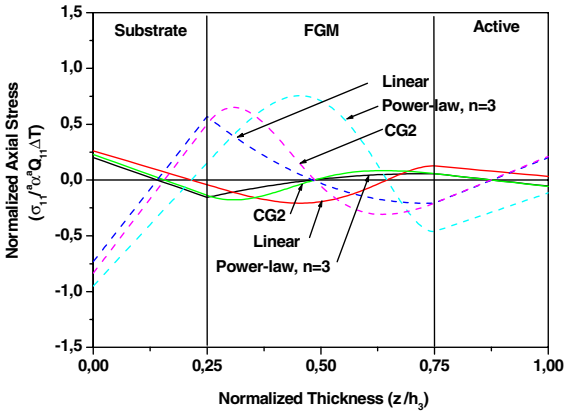

Figure 11. The normalized axial stress distribution under a thermal field (dashed curves) and combined electrical and thermal fields (solid curves).

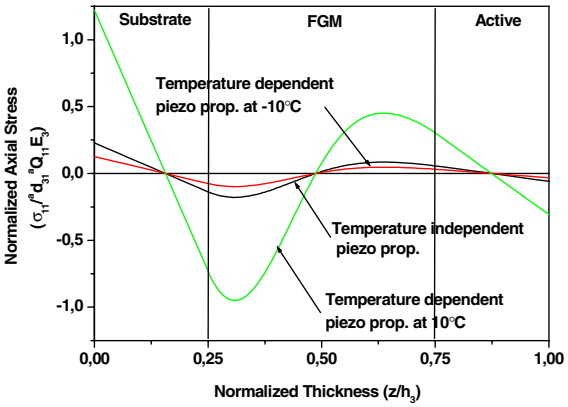

Figure 12. The effect of the temperature dependence of the piezoelectric properties on the stress characteristics in CG2 FGM.

stress characteristics. The Curie temperature of PZT5H is between 170–190 °C and the piezoelectric properties degrade rapidly in this temperature range. As per [31], the temperature-dependent piezo strain term ($\bar{d}_{31}$) for PZT5H is taken as -1.16 pm V^{-1} C^{-1}, which is valid in the range -70 to 100 °C. The stress distribution in the material is presented for ΔT equal to -10 and 10 °C. As seen from figure 12, higher stresses are induced in the material at temperatures higher than reference temperature (25 °C) due to the additional strain term. Likewise, the stresses are reduced at lower temperature. Subsequently, the actuation capability (i.e. the induced forces) will be affected and the effect will be linear due to the linear dependence of the piezo strain coefficients. Due to the dependence of the piezoelectric strain coefficients on temperature, a graded piezo transducer can be realized by superposing a thermal gradient between the top and bottom surfaces of the piezoelectric material.

5. Summary and conclusions

This paper discusses the stress characteristics for electro-thermo-elastically graded materials under electrical and thermal excitations with temperature-dependent electrical properties. A uniaxial model is presented and exact solutions for symmetric as well as asymmetric material layer structures are derived based on Euler–Bernoulli theory. Non-dimensional graphs are presented for the qualitative description of stresses over material thickness.

- A large difference in the elastic properties of the constituent material phases results in a stress distribution with steep gradients near the stiffer material. As the nature of the stress depends on the polarity of the applied electrical field, high tensile stress may be induced near the stiffer material. This situation needs critical evaluation, especially under dynamic conditions where repeatedly alternating stresses may lead to fatigue and subsequently fracture of the material.
- The power-law-based compositional gradations, which are incomplete polynomials, result in high stress gradients at the interfaces of the FG layer. The interfacial stress gradients are completely avoided by employing CG2. Owing to C^1-*continuity*, CG2 not only eliminates stress gradients at the interfaces but also reduces the maximum gradient occurring over the thickness of the material.
- The actuation authority of the graded material is significantly influenced by the modular ratio and the compositional variation. While CG2 gradation performs better *vis-à-vis* linear gradation for softer substrates, the latter proves superior for stiff substrates. It will be an interesting problem to optimize the compositional variation to include merits of both the variations.
- The inclusion of thermal effects in the model is important in order to predict the behaviour of the graded material at temperatures away from the reference temperatures. The temperature dependence of piezoelectric properties plays an important role by either augmenting or reducing the actuation efficiency of the system. It would be worthwhile to obtain the response of active FGM under arbitrarily varying temperature distribution over the material thickness.
- Our future work will focus on developing a generic FGM model that includes remnant polarization and strain effects and non-linear material behaviour. Remnant effects in the active material are important under high electric fields, while non-linear behaviour of the passive phase may play an important role in the thermal regime, e.g. the viscoelastic effect may become important for soft substrates. The direct piezoelectric effect formulated in this paper will be suitably modified to include the above-mentioned effects, and the sensor characteristics will be reported soon.

Acknowledgments

Financial support from the Indo-German cooperation programme under project IND 99/043 is gratefully acknowledged.

References

[1] Suresh S and Mortensen A 1998 *Fundamentals of Functionally Graded Materials* (London: IOM Communications)
[2] Suresh S 2001 Graded materials for resistance to contact deformation and damage *Science* **292** 2447–51

[3] Suresh S, Olsson M, Giannakopoulos A, Padture N P and Jitcharoen J 1999 Engineering the resistance to sliding-contact damage through controlled gradients in elastic properties at contact surfaces *Acta Mater.* **47** 3915–26

[4] Freund L B 1996 Some elementary connections between curvature and mismatch strain in compositionally graded thin films *J. Mech. Phys. Solids* **44** 723–6

[5] Reddy J N 2000 Analysis of functionally graded plates *Int. J. Numer. Methods Eng.* **47** 663–84

[6] Suresh S, Giannakopoulos A and Olsson M 1994 Elastoplastic analysis of thermal cycling: layered materials with sharp interfaces *J. Mech. Phys. Solids* **42** 979–1018

[7] Finot M and Suresh S 1996 Small and large deformation of thick and thin-film multi-layers: effects of layer geometry, plasticity and compositional gradients *J. Mech. Phys. Solids* **44** 683–721

[8] Han X, Liu G R and Lam K Y 2001 Transient waves in plates of functionally graded materials *Int. J. Numer. Methods Eng.* **52** 851–65

[9] Li Y, Ramesh K T and Chin E S C 2001 Dynamic characterization of layered and graded structures under impulsive loading *Int. J. Solids Struct.* **38** 6045–61

[10] Butcher R J, Rousseau C-E and Tippur H V 1999 A functionally graded particulate composite: preparation, measurements and failure analysis *Acta Mater.* **47** 259–68

[11] Suresh S, Giannakopoulos A and Alcala J 1997 Spherical indentation of compositionally graded materials: theory and experiments *Acta Mater.* **45** 1307–21

[12] Nakamura T, Wang T and Sampath S 2000 Determination of properties of graded materials by inverse analysis and instrumented indentation *Acta Mater.* **48** 4293–306

[13] Liu G R, Han X, Xu Y G and Lim K Y 2001 Material characterization of functionally graded material by means of elastic waves and a progressive-learning neural network *Compos. Sci. Technol.* **61** 1401–11

[14] Liu G R, Han X and Lim K Y 2002 A combined genetic algorithm and nonlinear least squares method for material characterization using elastic waves *Comput. Methods Appl. Mech. Eng.* **191** 1909–21

[15] Gasik M M 1998 Micromechanical modeling of functionally graded materials *Comput. Mater. Sci.* **13** 42–55

[16] Weissenbek E, Pettermann H and Suresh S 1997 Elasto-plastic deformation of compositionally graded metal-ceramic composites *Acta Mater.* **45** 3401–17

[17] Starzewski M, Jasiuk I, Wang W and Alzebdeh K 1996 Composites with functionally graded interphases: mesocontinuum concept and effective transverse conductivity *Acta Mater.* **44** 2057–66

[18] Schmauder S and Weber W 2001 Modelling of functionally graded materials by numerical homogenization *Arch. Appl. Mech.* **71** 182–92

[19] Pitakthangphong S and Busso E P 2002 Self-consistent elasto-plastic stress solutions for functionally graded material systems subjected to thermal transients *J. Mech. Phys. Solids* **50** 695–716

[20] Yamada K, Ohkubo A and Nakamura K 2001 Functional grading of a piezoelectric 1-3 composite for ultrasonic transducers with enhanced axial and lateral resolution *Proc. Symp. IEEE Ultrasonics (Atlanta, October 2001)* (Piscataway, NJ: IEEE) pp 1031–4

[21] Chatterjee D K, Ghosh S K and Furlani E P 1999 Controlled composition and crystallographic changes in forming functionally gradient piezoelectric transducer *US Patent Specification* 5,900,274

[22] Ruys A J, Popov E B, Sun D, Russell J J and Murray C C J 2001 Functionally graded electrical/thermal ceramic systems *J. Eur. Ceram. Soc.* **21** 2025–9

[23] Pei Y T and De Hosson J 2000 Functionally graded materials produced by laser cladding *Acta Mater.* **48** 2617–24

[24] Liu G R and Tani J 1992 SH surface waves in functionally gradient piezoelectric material plates *Trans. Japan Soc. Mech. Eng.* A **58** 504–7

[25] Liu G R and Tani J 1994 Surface waves in functionally gradient piezoelectric material plates *ASME J. Vib. Acoust.* **116** 440–8

[26] Zhu X, Xu J, Meng Z, Jianming Z, Zhou S, Li Q, Liu Z and Ming N 2001 Microdisplacement characteristics and microstructures of functionally graded piezoelectric ceramic actuator *Mater. Des.* **21** 561–6

[27] Reddy J N and Cheng Z-Q 2001 Three-dimensional solutions of smart functionally graded plates *Trans. ASME, J. Appl. Mech.* **68** 234–41

[28] Ng T Y, He X Q and Liew K M 2002 Finite element modeling of active control of functionally graded shells in frequency domain via piezoelectric sensors and actuators *Comput. Mech.* **28** 1–9

[29] Lim C W and He L H 2001 Exact solution of a compositionally graded piezoelectric layers under uniform stretch, bending and twisting *Int. J. Mech. Sci.* **43** 2479–92

[30] Almajid A, Taya M and Hudnut S 2001 Analysis of out-of-plane displacement and stress field in a piezocomposite plate with functionally graded microstructure *Int. J. Solids Struct.* **38** 3377–91

[31] Wang D, Fotinich Y and Carman G P 1998 Influence of temperature on the electromechanical and fatigue behavior of piezoelectric ceramics *J. Appl. Phys.* **83** 5342–50

[32] Hooker M W 1998 Properties of PZT-based piezoelectric ceramics between −150 and 250 °C NASA/CR-1998-208708

[33] Aboudi J 2000 Micromechanical prediction of the effective behavior if fully coupled electro-magneto-thermo-elastic multiphase composites NASA/CR-2000-209787

[34] Aboudi J, Pindera M-J and Arnold S M 2002 High-fidelity generalization method of cells for inelastic periodic multiphase materials NASA/TM-2002-211469